

## Exotic Molecular States in $^{12}\text{Be}$

M. Freer,<sup>1,2</sup> J. C. Angélique,<sup>2</sup> L. Axelsson,<sup>3</sup> B. Benoit,<sup>4</sup> U. Bergmann,<sup>5</sup> W. N. Catford,<sup>6</sup> S. P. G. Chappell,<sup>7</sup> N. M. Clarke,<sup>1</sup> N. Curtis,<sup>6</sup> A. D'Arrigo,<sup>4</sup> E. de Goes Brennard,<sup>4</sup> O. Dorvaux,<sup>8</sup> B. R. Fulton,<sup>1</sup> G. Giardina,<sup>9</sup> C. Gregori,<sup>10</sup> S. Grévy,<sup>11,\*</sup> F. Hanappe,<sup>4</sup> G. Kelly,<sup>12</sup> M. Labiche,<sup>2</sup> C. Le Brun,<sup>2</sup> S. Leenhardt,<sup>11</sup> M. Lewitowicz,<sup>13</sup> K. Markenroth,<sup>3</sup> F. M. Marqués,<sup>2</sup> M. Motta,<sup>9</sup> J. T. Murgatroyd,<sup>1</sup> T. Nilsson,<sup>3,†</sup> A. Ninane,<sup>2,‡</sup> N. A. Orr,<sup>2</sup> I. Piqueras,<sup>10</sup> M. G. Saint Laurent,<sup>13</sup> S. M. Singer,<sup>1</sup> O. Sorlin,<sup>11</sup> L. Stuttgé,<sup>8</sup> and D. L. Watson<sup>14</sup>

<sup>1</sup>*School of Physics and Astronomy, University of Birmingham, Edgbaston, Birmingham B15 2TT, United Kingdom*

<sup>2</sup>*Laboratoire de Physique Corpusculaire, ISMRA and Université de Caen, IN2P3-CNRS, 14050 Caen Cedex, France*

<sup>3</sup>*Fysiska Institutionen, Chalmers Tekniska Högskola, S-412 96 Göteborg, Sweden*

<sup>4</sup>*Université Libre de Bruxelles, CP 226, B-1050 Bruxelles, Belgium*

<sup>5</sup>*Det Fysiske Institut, Aarhus Universitet, DK 8000 Aarhus C, Denmark*

<sup>6</sup>*Department of Physics, University of Surrey, Guildford, Surrey GU2 5XH, United Kingdom*

<sup>7</sup>*Nuclear and Astrophysics Laboratory, University of Oxford, Keble Road, Oxford OX1 3RH, United Kingdom*

<sup>8</sup>*Institut de Recherches Subatomique, IN2P3-CNRS/Université Louis Pasteur, BP 28, 67037 Strasbourg Cedex, France*

<sup>9</sup>*Istituto Nazionale di Fisica Nucleare, Sezione di Catania and Dipartimento di Fisica, Università di Messina, Messina, Italy*

<sup>10</sup>*Instituto Estructura de la Materia, CSIC, E-28006 Madrid, Spain*

<sup>11</sup>*Institut de Physique Nucléaire, IN2P3-CNRS, 91406 Orsay Cedex, France*

<sup>12</sup>*School of Sciences, Staffordshire University, College Road, Stoke-on-Trent ST4 2DE, United Kingdom*

<sup>13</sup>*GANIL (CEA/DSM-CNRS/IN2P3), BP 5027, 14076 Caen Cedex, France*

<sup>14</sup>*Department of Physics, University of York, York YO1 5DD, United Kingdom*

(Received 11 August 1998)

The breakup of  $^{12}\text{Be}$  into  $^6\text{He} + ^6\text{He}$  and  $^4\text{He} + ^8\text{He}$  has been studied using a 378 MeV  $^{12}\text{Be}$  beam inelastically excited by  $^{12}\text{C}$  and  $(\text{CH}_2)_n$  targets. The measurements indicate that breakup occurs from rotational states in the 10 to 25 MeV excitation energy interval, with spins in the range of  $4\hbar$  to  $8\hbar$ . The inferred moment of inertia is consistent with the cluster decay of an exotic molecular structure in  $^{12}\text{Be}$ , which may be associated with an  $\alpha$ -4n- $\alpha$  cluster configuration. [S0031-9007(99)08451-3]

PACS numbers: 21.10.Hw, 21.60.Gx, 25.70.Ef, 27.20.+n

The understanding of the covalent binding of the  $\text{H}_2$  molecule by Heitler and London [1] via the exchange interaction was a landmark discovery as it not only provided a mechanism for the binding of a large class of molecules but was also a triumph for quantum mechanics. More recently, it has been speculated that very similar molecular-type structures could be observed in nuclei. Wilkinson, for example, devised ring and chain structures of alpha particles *covalently* bound by valence neutrons [2]. Additionally, following the pioneering theoretical studies of nuclear molecules of Seya *et al.* [3], systematic evidence for nuclear dimers in  $^{9-11}\text{Be}$  and  $^{9-11}\text{B}$  has been identified by von Oertzen [4,5]. As an example of such molecular behavior, the  $^9\text{Be}$  ground state may be understood in terms of the 3-body  $\alpha$ -n- $\alpha$  molecular structure. If the neutron is removed then the remaining two alpha particles dissociate as  $^8\text{Be}$  is unbound to  $\alpha$  decay. This is analogous to the binding of the  $\text{H}_2^+$  molecule where the removal of the electron results in two unbound protons. In systems such as  $^9\text{Be}$ , the potential in which the valence neutron resides is strongly influenced by the underlying  $\alpha$ -particle structure, and thus its wave function is two centered. Densities calculated using the antisymmetrized molecular dynamics (AMD) description also reveal molecularlike shapes in many light nuclei [6].

These ideas can be extended to very neutron-rich nuclei, such as the  $\alpha$ -4n- $\alpha$  system  $^{12}\text{Be}$ , where a well developed molecular structure is predicted for excited states [5]. Further, the nuclei  $^6\text{He}$  and  $^8\text{He}$  can be characterized in terms of their  $\alpha$ -Xn cluster structure [7]. Hence, the decay of a " $^{12}\text{Be}$  molecule" into the exotic cluster components,  $^6\text{He} + ^6\text{He}$  or  $^8\text{He} + ^4\text{He}$ , may be possible. Preliminary indications of such structures have been inferred from a measurement of  $p + ^{12}\text{Be}$  inelastic scattering [8]. The present paper reports on a study of the He-cluster decay modes of  $^{12}\text{Be}$ .

A 378 MeV  $^{12}\text{Be}$  secondary beam, with an energy spread of 18 MeV and intensity  $2 \times 10^4$  particles per second, was produced from a 63 MeV per nucleon primary  $^{18}\text{O}$  beam of intensity  $2 \mu\text{A}$ , provided by the GANIL coupled cyclotrons, incident on a 200-mg  $\text{cm}^{-2}$ -thick beryllium target. Beam purification ( $\sim 95\%$   $^{12}\text{Be}$ ) was achieved using the LISE3 spectrometer. The beam was tracked onto 10 mg  $\text{cm}^{-2}$   $^{12}\text{C}$  and 20 mg  $\text{cm}^{-2}$   $(\text{CH}_2)_n$  target foils, using two x-y position sensitive parallel plate avalanche counters. The breakup products from the ( $^{12}\text{Be}, ^6\text{He}^6\text{He}$ ) and ( $^{12}\text{Be}, ^4\text{He}^8\text{He}$ ) reactions, on proton and  $^{12}\text{C}$  targets, were detected in an array of ten Si-CsI telescopes. The Si elements were 500- $\mu\text{m}$ -thick  $5 \times 5 \text{ cm}^2$  two-dimensional position sensitive detectors. These were backed by 4.0-cm-thick CsI detectors. The

detectors were arranged in a symmetric fashion around the beam axis to pick up breakup fragments in opposing telescopes. The  $^4\text{He}$ ,  $^6\text{He}$ , and  $^8\text{He}$  reaction products were identified from their characteristic energy loss in the Si-CsI telescopes. Using the measurements of the mass, energy, and emission angle of the fragments, the energy of the undetected recoil was calculated via momentum conservation, and the reaction  $Q$  value was obtained. In the case of reactions on the  $(\text{CH}_2)_n$  target, the ambiguity in the target nucleus led to an uncertainty in the mass of the recoil. Figure 1a shows the  $Q$ -value spectrum reconstructed for  $^6\text{He} + ^6\text{He}$  coincidences assuming the reaction  $^{12}\text{C}(^{12}\text{Be}, ^6\text{He}^6\text{He})$  ( $Q = -10$  MeV). The bold histogram corresponds to reactions from the natural carbon target (denoted  $^{12}\text{C}_{\text{nat}}$ ), and the narrow-lined histogram corresponds to reactions from the  $(\text{CH}_2)_n$  target producing two  $^6\text{He}$  nuclei, assuming a  $^{12}\text{C}$  recoil. The peaks in these spectra at  $Q = -10$  MeV indicate that the  $^{12}\text{C}(^{12}\text{Be}, ^6\text{He}^6\text{He})$  reaction has been correctly identified. The inset displays Monte Carlo simulations of the reaction process in the case of the  $(\text{CH}_2)_n$  target. These simu-

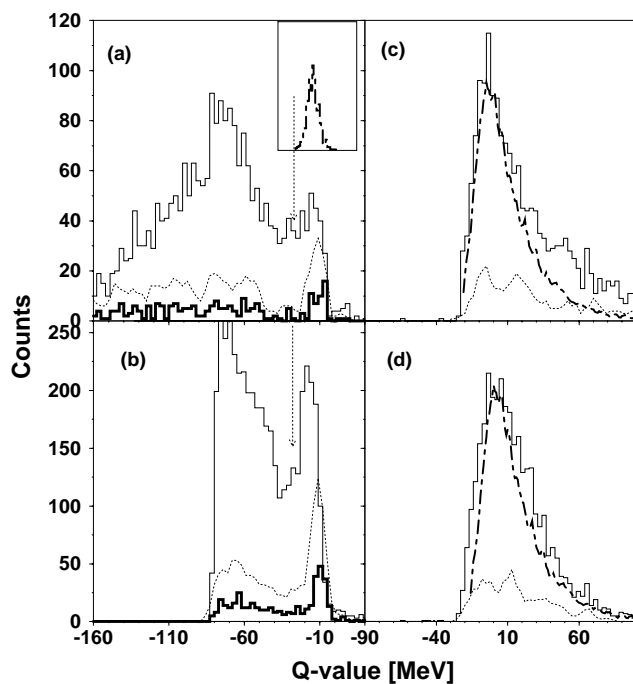


FIG. 1.  $Q$ -value spectra for the reactions (a)  $^{12}\text{C}(^{12}\text{Be}, ^6\text{He}^6\text{He})$ , (b)  $^{12}\text{C}(^{12}\text{Be}, ^4\text{He}^8\text{He})$ , (c)  $p(^{12}\text{Be}, ^6\text{He}^6\text{He})$ , and (d)  $p(^{12}\text{Be}, ^4\text{He}^8\text{He})$  from the  $(\text{CH}_2)_n$  target. The arrows indicate the  $Q$  value used to discriminate between the two target components. The bold histograms in (a) and (b) are for the reactions from the  $^{12}\text{C}_{\text{nat}}$  target. The dotted curves in (a)–(d) correspond to the  $^{12}\text{C}_{\text{nat}}$  target data scaled to account for differences in beam exposure and thickness of the two targets and in (c) and (d) indicate the level of background in these spectra. The dot-dashed curves in (c) and (d) represent the results of Monte Carlo simulations of the reactions from the proton target. The inset in (a) shows the result of the simulation for the  $^{12}\text{C}(^{12}\text{Be}, ^6\text{He}^6\text{He})$  reaction for the  $(\text{CH}_2)_n$  target.

lations include the effects of the position and energy resolutions of the detectors, energy and angular spread of the beam, and energy and angular straggling of the beam and reaction products in the target, and suggest a  $Q$ -value resolution of 3.5 MeV for the  $^{12}\text{C}_{\text{nat}}$  target and 9 MeV for the  $(\text{CH}_2)_n$  target, in agreement with the data. The dotted line is an indication of the background contribution to the  $(\text{CH}_2)_n$  target data. This clearly demonstrates that there are additional  $^6\text{He} + ^6\text{He}$  coincidences produced from the  $^1\text{H}$  component of the  $(\text{CH}_2)_n$  target. The simulations indicate that the proton recoil data extend into the region under the peak identified with the  $^{12}\text{C}(^{12}\text{Be}, ^6\text{He}^6\text{He})$  reaction. This indicates that the reactions from the proton and  $^{12}\text{C}$  components of the  $(\text{CH}_2)_n$  target are not completely resolved.

Figure 1c shows the data in Fig. 1a reconstructed assuming the reaction  $p(^{12}\text{Be}, ^6\text{He}^6\text{He})$ ; in the instance that an event was associated with the peak at  $Q \approx -10$  MeV in Fig. 1a (indicated by the arrow), the spectrum in Fig. 1c was not incremented. The bold dot-dashed line in Fig. 1c displays the results of Monte Carlo simulations for the  $p(^{12}\text{Be}, ^6\text{He}^6\text{He})$  reaction, normalized to the data. The simulations reproduce the shape of the spectrum, including the high energy tail. The poorer resolution (26 MeV) is due to the larger recoil energy carried away by the protons. The dotted line in Fig. 1c again shows the scaled  $^{12}\text{C}_{\text{nat}}$  target data, suggesting that the background contribution to the  $Q$ -value spectrum is of the order of 10% to 20%, demonstrating that this spectrum is dominated by events from the  $p(^{12}\text{Be}, ^6\text{He}^6\text{He})$  reaction. Figures 1b and 1d display the results of similar analyses for the  $^4\text{He} + ^8\text{He}$  coincidences assuming the  $^{12}\text{C}(^{12}\text{Be}, ^4\text{He}^8\text{He})$  and  $p(^{12}\text{Be}, ^4\text{He}^8\text{He})$  reactions, respectively. These  $Q$ -value spectra show that  $^4\text{He} + ^8\text{He}$  coincidences arising from the breakup of  $^{12}\text{Be}$  are produced in reactions from both the  $^{12}\text{C}$  and  $p$  targets.

The excitation energy of the  $^{12}\text{Be}$  nucleus has been calculated from the relative velocity of the two breakup fragments. The spectrum shown in Fig. 2a corresponds to combined data from all the targets for the  $^6\text{He} + ^6\text{He}$  breakup. The  $^8\text{He} + ^4\text{He}$  breakup data are shown separately for the two  $Q \approx -10$  MeV peaks in Fig. 1b (Fig. 2b) and Fig. 1d (Fig. 2c). The dotted histogram in Fig. 2a shows the spectrum of  $^{12}\text{Be}$  excited states reconstructed from events associated with only the peak at  $Q \approx -10$  MeV in Fig. 1a, that is, events arising primarily from  $^{12}\text{Be}$  breakup on  $^{12}\text{C}$ . These data suggest that for the  $^6\text{He} + ^6\text{He}$  channel there are a number of states in the range  $10 < E_x < 25$  MeV (Table I). The widths are consistent with the experimental resolution of 0.8 MeV, as predicted by the simulations. The structure in the  $^8\text{He} + ^4\text{He}$  spectra is not so striking. This may result from the higher multiplicity of states that can feed this breakup channel. As the decay into two spin zero  $^6\text{He}$  nuclei results in the production of identical bosons, then symmetry arguments dictate that only even spin states can

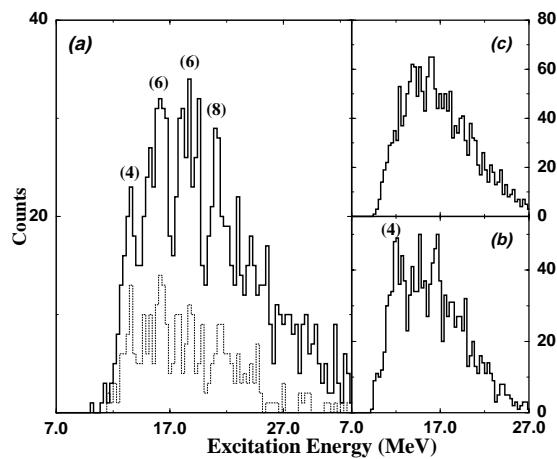


FIG. 2. The reconstructed  $^{12}\text{Be}$  excitation energy spectra (a)  $^{12}\text{Be} \rightarrow ^6\text{He} + ^6\text{He}$  for proton plus carbon recoils, (b)  $^{12}\text{Be} \rightarrow ^8\text{He} + ^4\text{He}$  for carbon recoils, and (c)  $^{12}\text{Be} \rightarrow ^8\text{He} + ^4\text{He}$  for proton recoils. The dotted histogram in (a) represents  $^6\text{He} + ^6\text{He}$  decay events identified with the  $Q = -10$  MeV peak in Fig. 1a and, hence, is dominated by events with carbon recoils.

feed this channel, whereas both odd and even spin states may be observed in the  $^8\text{He} + ^4\text{He}$  decay. A comparison of the energies of the states in the  $^6\text{He} + ^6\text{He}$  spectra and the  $^8\text{He} + ^4\text{He}$  data from the  $^{12}\text{C}$  target indicates that many of the states in the two decay channels may be the same (Table I).

It is possible to extract spin information from the angular correlations of the reaction products. The reaction yields may be parametrized in terms of two angles,  $\theta^*$  and  $\psi$ , where  $\theta^*$  is the center-of-mass scattering angle of the  $^{12}\text{Be}$  nucleus, and  $\psi$  is the emission angle of the breakup products in the  $^{12}\text{Be}$  center-of-mass frame, with both angles measured with respect to the beam direction. The angular correlations for reactions with spin zero breakup products take the form of ridges in the  $\theta^*$ - $\psi$  plane that are characterized by the function  $|P_J(\cos[\psi + a\theta^*])|^2$ .  $J$  is the spin of the  $^{12}\text{Be}$  excited state and the phase shift  $a$  corresponds to the ratio  $(l_f/J)$  of the final state grazing angular momentum to the spin  $J$ . The periodicity and gradient of the ridge structures are thus characteristic of the spin of the breakup state. Previous studies [9,10] have shown that it is possible to relate the entrance and exit channel angular momenta via  $l_i = l_f + J$ . Hence, a reaction model calculation of  $l_i$  may then be used to

predict the correlation gradient as a function of  $J$ . An independent analysis of the periodicity and gradient of the correlations provides consistent spin assignments. A discussion of the treatment of angular correlations may be found in [9]. The results of the correlation analysis of the present data are displayed in Fig. 3, where the data for several states in the  $^6\text{He} + ^6\text{He}$  channel have been projected onto the  $\theta^* = 0$  axis. To enhance the statistical significance of the correlations, the  $^1\text{H}$ - and  $^{12}\text{C}$ -recoil data have been combined. For each event a  $^{12}\text{C}$  or  $^1\text{H}$  recoil was assumed, according to the  $Q$ -value cut shown in Fig. 1a, and then the angles  $\theta^*$  and  $\psi$  could be correctly reconstructed. For the  $^{12}\text{C} + ^{12}\text{Be}$  reaction the acceptance of the detection system limits the angular coverage to  $\theta^* < 10^\circ$ . Calculated angular correlations, generated from the reaction amplitudes predicted by a coupled channels reaction code [11], suggest that over this limited interval the angular correlations are not strongly affected by the projection onto the  $\theta^* = 0$  axis and are characterized by the function  $|P_J(\cos\psi)|^2$ . The periodicity of these data thus provide a model independent spin determination. However, for the  $p + ^{12}\text{Be}$  reactions the center-of-mass angular coverage is larger,  $\theta^* < 180^\circ$ . Thus, the data must be projected along the ridges in order to preserve the correlation structure. The coupled channels calculations suggest that for the  $p + ^{12}\text{Be}$  reaction  $l_i = (6-7)\hbar$ , and, thus, the projection angle is determined by the ratio  $(l_i - J)/J$ . The data in Fig. 3a correspond to the 13.2 MeV state, and for the proton target they have been projected at an angle which corresponds to  $J = 4$ , implied by the periodicity of the correlation. It is also important to consider the fraction of events from the  $p(^{12}\text{Be}, ^6\text{He}^6\text{He})$  reaction which are misidentified as arising from interactions with the  $^{12}\text{C}$  component of the  $(\text{CH}_2)_n$  target. This corresponds to the interval  $\theta^* < 28^\circ$  for the  $p(^{12}\text{Be}, ^{12}\text{Be}^*)$  reaction. The reconstruction of  $\theta^*$  assuming a  $^{12}\text{C}$  recoil compresses these data into the interval  $\theta^* < 2.3^\circ$ . For the  $J = 4$  state the phase shift is comparable with that calculated for the  $^{12}\text{C}(^{12}\text{Be}, ^{12}\text{Be}^*)$  reaction. Thus, these data should also follow the  $|P_J(\cos\psi)|^2$  trend. Figures 3b and 3d show the correlations for the peaks at  $E_x = 16.1$  and 22.8 MeV projected perpendicular to the  $\psi$  axis compared with Legendre polynomials of order 6 and 8, as the value of  $l_i = (6-7)\hbar$  and spins  $J = 6$  and 8 implies that, to first order, the correlations would be independent of  $\theta^*$ .

TABLE I. Excitation energies and deduced spins of states observed in the  $^6\text{He} + ^6\text{He}$  and  $^8\text{He} + ^4\text{He}$  decay channels. The absolute uncertainty in the excitation energies is 0.5 MeV and the typical statistical uncertainty is  $< 0.4$  MeV. Brackets indicate tentative energy assignments.

$^6\text{He} + ^6\text{He}$	$E_x$ (MeV)	13.2	14.9	16.1	17.8	18.6	19.3	20.9	22.8	(24.0)	(25.1)
	$J$	4		6	6			8			
$^8\text{He} + ^4\text{He}$	$E_x$ (MeV)	12.1	13.0	13.9	14.7	(15.4)	16.6	(17.7)	(18.4)	(19.3)	20.8
	$J$	4									

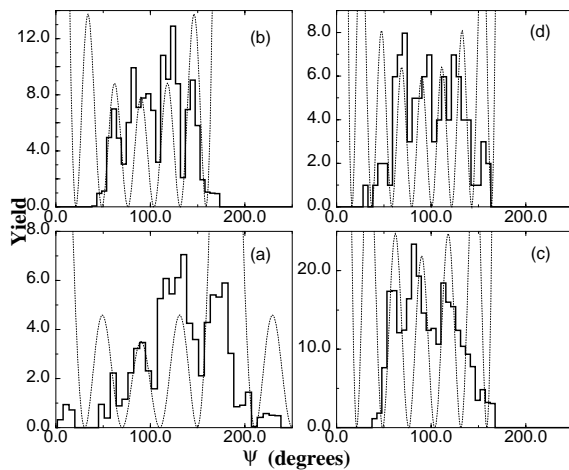


FIG. 3. Projected angular correlations (see text) for the states at (a) 13.2 MeV ( $J = 4$ ), (b) 16.1 MeV ( $J = 6$ ), (c) triplet centered at 18.6 MeV ( $J = 6$ ), and (d) 20.9 MeV ( $J = 8$ ). The dotted lines correspond to the  $|P_J|^2$ , where  $J$  is the assigned spin.

Figure 3c represents the projection of the correlation for the group of states between 17.8 and 19.3 MeV and indicates a dominant  $J = 6$  contribution. A similar analysis for the  ${}^8\text{He} + {}^4\text{He}$  state at 13.0 MeV also indicates  $J = 4$ , while for other states the correlations are not conclusive.

The energy-spin characteristics of the  ${}^6\text{He} + {}^6\text{He}$  breakup states are displayed in Fig. 4; the solid line is a fit to the data points. The gradient ( $\hbar^2/2I$ ) and intercept of the fit are  $0.15(\pm 0.04)$  MeV and  $10.8(\pm 1.8)$  MeV, respectively. This gradient can be compared with that predicted for a spherical  ${}^{12}\text{Be}$  nucleus and that for two

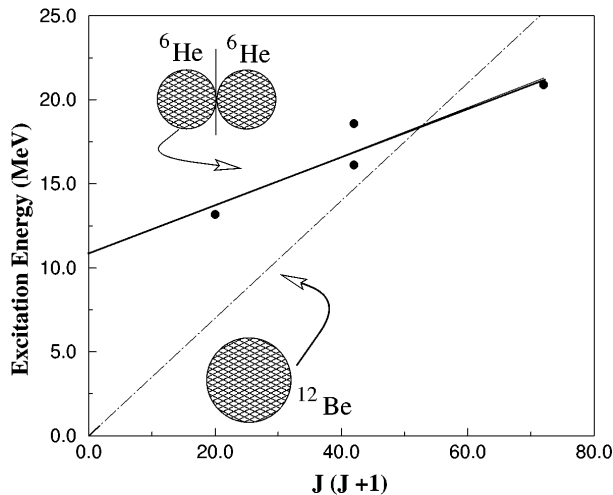


FIG. 4. The energy-spin systematics of the  ${}^6\text{He} + {}^6\text{He}$  breakup states (black dots). The solid line is a linear fit to the four points, and the dot-dashed line shows the extrapolated trajectory of a ground state band with a rotational energy of 350 keV.

touching  ${}^6\text{He}$  nuclei, with radii given by  $r = 1.3A^{1/3}$  fm,  $\hbar^2/2I = 360$  and 165 keV, respectively. The first  $2^+$  state in  ${}^{12}\text{Be}$  lies at 2.1 MeV which, if rotational, would imply  $\hbar^2/2I = 350$  keV (dot-dashed line), suggesting a small ground state deformation in agreement with AMD predictions [6,12]. In contrast, the gradient of the present data is consistent with a deformed  ${}^6\text{He} + {}^6\text{He}$  “molecule.” In accordance with the ideas developed by Ikeda [13] to describe  $\alpha$  clustering in light nuclei, such structures might be expected to appear close to the decay threshold, i.e., 10.1 MeV, in agreement with the observed intercept.

The work presented here thus provides evidence for a deformed, exotic  ${}^6\text{He} + {}^6\text{He}$  cluster structure in  ${}^{12}\text{Be}$ . This may be linked to an  $\alpha$ - $4n$ - $\alpha$  molecule. However, measurements of partial decay widths are required to confirm this connection.

The authors are grateful to the technical and operations staffs of LPC and GANIL. This work was funded by the EPSRC (U.K.) and the IN2P3-CNRS (France). Additional support was provided by the ALLIANCE Programme of the British Council and the Ministère des Affaires Etrangères, and the Human Capital and Mobility Programme of the European Community (Contract No. CHGE-CT94-0056).

\*Present address: Laboratoire de Physique Corpusculaire, ISMRA et Université de Caen, IN2P3-CNRS, Bd Maréchal Juin, 14050 Caen Cedex, France.

†Present address: ISOLDE, PPE-Division, CERN, CH-1211 Geneve 23, Switzerland.

‡On leave from Institut de Physique, Université Catholique de Louvain, Louvain-la-Neuve, Belgium.

- [1] W. Heitler and F. London, *Z. Phys.* **44**, 455 (1927).
- [2] D. H. Wilkinson, *Nucl. Phys.* **A452**, 296 (1986).
- [3] M. Seya, M. Kohno, and S. Nagata, *Prog. Theor. Phys.* **65**, 204 (1981).
- [4] W. von Oertzen, *Z. Phys. A* **354**, 37 (1996).
- [5] W. von Oertzen, *Z. Phys. A* **357**, 355 (1997).
- [6] Y. Kanada-En'yo and H. Horiuchi, *Phys. Rev. C* **52**, 628 (1995); A. Doté, H. Horiuchi, and Y. Kanada-En'yo, *Phys. Rev. C* **56**, 1844 (1997).
- [7] J. Wurzer and H. M. Hofmann, *Phys. Rev. C* **55**, 688 (1997), and references therein.
- [8] A. A. Korshinnikov *et al.*, *Phys. Lett. B* **343**, 53 (1995).
- [9] M. Freer, *Nucl. Instrum. Methods Phys. Res., Sect. A* **383**, 463 (1996).
- [10] W. D. M. Rae and R. K. Bhowmik, *Nucl. Phys.* **A420**, 320 (1984).
- [11] N. M. Clarke, coupled channels computer code CHUCK97, University of Birmingham.
- [12] H. Horiuchi and Y. Kanada-En'yo, *Nucl. Phys.* **A616**, 394c (1997).
- [13] K. Ikeda, *Suppl. Prog. Theor. Phys. (Japan) Extra Numbers*, 464 (1968).